



# A unified integral theory of laminar natural convection over surfaces at arbitrary inclination from horizontal to vertical



Abhijit Guha, Kaustav Pradhan\*

Mechanical Engineering Department, Indian Institute of Technology Kharagpur, Kharagpur, 721302, India

## ARTICLE INFO

### Article history:

Received 16 February 2016

Received in revised form

12 August 2016

Accepted 12 August 2016

### Keywords:

Natural convection

Inclined surface

Integral analysis

Physical mechanisms

## ABSTRACT

Similarity analysis shows that  $Nu_x$  varies as  $Gr_x^{1/4}$  for natural convection on an isothermal vertical surface but  $Nu_x$  varies as  $Gr_x^{1/5}$  for isothermal horizontal surfaces. It is thus difficult to develop a rigorously-derived, closed-form solution for  $Nu_x$  on a surface with arbitrary inclination. In the present study we have formulated, for the first time, a unified integral theory for laminar natural convection on an arbitrarily inclined surface, both for specified variation in surface temperature ( $T_w(x) = T_\infty + f_1(x)$ ) and surface heat flux ( $q_w = f_2(x)$ ), such that the Nusselt number matches with results obtained from the similarity analysis in the limiting cases of vertical and horizontal surfaces. The predictions of the present formulation also agree well with previous computational and experimental results at intermediate angles of inclination between the vertical and the horizontal.  $f_1(x)$  or  $f_2(x)$  can be any arbitrary function, including power law variation, and represents a differentially heated surface. Another important feature of the present integral theory is that the developed generalized equations can accommodate arbitrary orders of polynomials ( $\lambda$  and  $\chi$ ) representing the velocity and temperature profiles, and optimum values for  $\lambda$  and  $\chi$  have been systematically determined for various boundary conditions (i.e.  $\lambda = 4$ ,  $\chi = 2$  for isothermal case and  $\lambda = 3$ ,  $\chi = 2$  for constant-heat-flux case). Because of the simplicity of the present theory, it is easy to generate results for combinations of Grashof number, Prandtl number and inclination angle not presented here. The different physical mechanisms for natural convection on vertical and horizontal surfaces (buoyancy versus indirect pressure difference) are explained with the help of the present analysis. It is shown that for moderate to high Prandtl number fluids, the natural convection mechanism for vertical surface is the dominating factor for a large range of inclination angles except for near horizontal configurations. The range of inclination angles for which the vertical solution predominates decreases as the Prandtl number decreases. For very low Prandtl number fluids at low Grashof number, the vertical mechanism applies only to nearly vertical surfaces. A physical explanation for such behaviour is discovered here, for the first time, in terms of the relative magnitudes of the buoyancy and indirect pressure difference. Compact scaling laws for significant data reduction are proposed and explained. New algebraic correlations have been developed that give Nusselt number as explicit functions of Grashof number, Prandtl number and inclination angle. A new methodology for the representation of the results brings out more powerfully the role of inclination angle in determining the heat transfer rate as well as the mechanism of natural convection.

© 2016 Elsevier Masson SAS. All rights reserved.

## 1. Introduction

Heat transfer by natural convection is an important physical phenomenon and is often encountered in engineering devices such as electronic equipments, nuclear reactors, etc. Therefore, the

phenomenon of natural convection has been extensively studied considering different geometries and different surface thermal conditions. For a vertical semi-infinite surface, natural convection has been studied using integral analysis [1–4], similarity analysis [1,5–7] and experiments [8]. For a horizontal semi-infinite surface, natural convection has been studied using integral analysis [9], series solutions [10], similarity analysis [11–15] and experiments [16,17]. Discussion on natural convection over vertical and horizontal surfaces is now a standard part of all books on convection

\* Corresponding author.

E-mail addresses: [a.guha@mech.iitkgp.ernet.in](mailto:a.guha@mech.iitkgp.ernet.in) (A. Guha), [kaustav.pradhan@mech.iitkgp.ernet.in](mailto:kaustav.pradhan@mech.iitkgp.ernet.in) (K. Pradhan).

Nomenclature		X	non-dimensional x coordinate
$a$	dimensional constant for $f_1(x)$ in specified variable surface temperature case	$y$	coordinate normal to the surface
$b$	a function of $Gr_x$ and $Pr$ used in Equation (34)	<i>Greek symbols</i>	
$c$	variable defined in Equation (34)	$\alpha$	thermal diffusivity
$f_1(x)$	function describing the temperature differential between surface and ambient	$\beta$	coefficient of volume expansion
$f_2(x)$	function for the specified surface heat flux	$\chi$	order of polynomial for temperature
$g$	acceleration due to gravity	$\Delta$	non-dimensional boundary layer thickness
$Gr_L$	Grashof number defined as $g\beta(T_w - T_\infty)L^3/\nu^2$	$\delta$	boundary layer thickness
$Gr_L^*$	modified Grashof number defined as $g\beta q_w L^4/k\nu^2$	$\delta_v$	velocity boundary layer thickness
$Gr_x$	local Grashof number defined as $g\beta(T_w - T_\infty)x^3/\nu^2$	$\delta_t$	thermal boundary layer thickness
$Gr_x^*$	modified local Grashof number $g\beta q_w x^4/k\nu^2$	$\varepsilon$	a small positive number
$h_x$	local heat transfer coefficient	$\gamma$	inclination angle from the horizontal
$k$	thermal conductivity of the fluid	$\lambda$	order of polynomial for velocity
$L$	reference length	$\mu$	dynamic viscosity
$n_1, n_2$	constants used in $Nu_x$ correlations	$\theta$	non-dimensional temperature
$Nu_x$	local Nusselt number, $h_x x/k$	$\rho$	density
$p$	pressure	$\nu$	kinematic viscosity
$Pr$	Prandtl number, $\nu/\alpha$	<i>Subscript</i>	
$q_w$	heat flux at the surface	$h$	horizontal surface
$T$	fluid temperature	$q$	constant heat flux case
$u$	velocity component parallel to the surface	$t$	isothermal case
$u_x$	velocity scale	$v$	vertical surface
$U$	non-dimensional $u$ velocity	$w$	value on the surface
$v$	velocity component normal to the surface	$x$	local value
$x$	coordinate along the surface	$\infty$	ambient condition

(e.g. Refs. [1–4]), and new results have appeared in recent publications ([9,14,15,18,19]). Reference [18] uses computational fluid dynamic (CFD) simulations to unearth new physical understanding of the effects of finiteness of a heated plate on the thermo-fluid-dynamics of natural convection above it. In Ref. [19], a CFD code is developed in-house to solve the highly non-linear coupled partial differential equations describing natural convection of non-Newtonian fluids on a horizontal plate.

Natural convective boundary layer flow over a horizontal surface is quite different from its counterpart on a vertical surface. In such buoyancy induced flows, the temperature gradient generating the buoyancy force does not directly cause the flow. It gives rise to a pressure gradient in the direction parallel to the surface, which is responsible for driving the convective flow. This is why Schlichting and Gersten [11] termed it as “indirect natural convection”, for which, unlike the usual analysis for the boundary layer, neither the term  $\partial p/\partial x$  nor the term  $\partial p/\partial y$  can be neglected. Similarity analysis shows that  $Nu_x$  varies as  $Gr_x^{1/4}$  for natural convection on an isothermal vertical surface but  $Nu_x$  varies as  $Gr_x^{1/5}$  for isothermal horizontal surfaces. In case of inclined surfaces, the natural convection mechanisms for both vertical and horizontal configurations are operative. It is thus difficult to develop a rigorously-derived, closed-form solution for  $Nu_x$  on a surface with arbitrary inclination, which will reduce to the known solutions in the two limits of horizontal and vertical surfaces.

In contrast to the extensive literature that exists for natural convection over horizontal or vertical surfaces, the literature available for inclined surfaces is rather limited. Rich and Burbank [20] gave experimental results (for air) for isothermal inclined surfaces, and, Vliet [21] gave experimental results (for water) for inclined surfaces subjected to constant heat flux. These experimental data were taken over certain ranges of inclination angles:

$50^\circ \leq \gamma \leq 90^\circ$  for [20] and  $30^\circ \leq \gamma \leq 85^\circ$  for [21]. Since natural convection on inclined surfaces does not admit similarity solution, previous studies have tried to relate the phenomenon on inclined surfaces to the limiting cases of vertical and horizontal surfaces. Rich and Burbank [20] and Vliet [21], for example, related their experimental results for inclined surfaces to that for the vertical surface by using the component of gravity parallel to the surface for calculating the Grashof number in their analysis. Pera and Gebhart [22] approximated the effect of a small inclination as a perturbation of flow over a horizontal surface. In contrast to these attempts [20–22] of relating to vertical or horizontal cases, a few studies have derived the non-similar boundary layer equations on an inclined surface and solved them using elaborate numerical techniques [23–25]. The formulation of Yu and Lin [23] holds true for the isothermal surface only, while the non-similar equations of Lin et al. [24] are valid for a constant surface heat flux only. The computation in both work [23,24] is performed in complex transformed co-ordinates. The numerical results of Chen et al. [25] are restricted to only two values of the Prandtl number ( $Pr = 0.7$  and  $Pr = 7$ ). Because of the complexities of the formulations and solution procedures of these previous theoretical studies [23–25], it is difficult to generate new numerical results for combinations of Grashof number, Prandtl number and inclination angle not presented in their work. Recently, Saha et al. [26] performed a scaling analysis for the natural convection of air past an inclined flat plate. Corcione et al. [27] considered natural convection on inclined plates where both sides of the plate are maintained at the same temperature.

Although the integral method has been extensively used for vertical or horizontal surfaces, to the best of the authors' knowledge, it has not been applied in the past for the study of inclined surfaces. The aim of the present work is to apply the integral

method to formulate a set of simple generic equations that can represent the natural convection on horizontal, inclined and vertical surfaces subjected to arbitrary variation in wall temperature or surface heat flux. With the help of this same set of equations, comprehensive calculations have been carried out to study the variation of Nusselt number as a function of Grashof number, Prandtl number and inclination angle ( $10^3 \leq Gr \leq 10^7$ ,  $0.01 \leq Pr \leq 100$  and  $0^\circ \leq \gamma \leq 90^\circ$ ). The prediction of the simple unified theory agrees well with previous experimental and computational results for whatever ranges of the parameters and boundary conditions they are available. A new, concise method of data representation sheds light on how the mechanism of natural convection on an inclined surface undergoes progressive changes as the inclination angle is varied from the horizontal to the vertical.

**2. Mathematical formulation**

Consider steady, laminar natural convection on a semi-infinite flat plate inclined at an acute angle  $\gamma$  to the horizontal. The plate is surrounded by a quiescent fluid which is at a temperature  $T_\infty$ . The  $x$  coordinate is measured from the leading edge of the plate and the  $y$  coordinate is measured normal to the plate. Gravity  $g$  acts vertically downwards, which is in the negative  $y$  direction for the horizontal plate orientation ( $\gamma = 0^\circ$ ). Two surface conditions are considered for the plate: (1) a specified variation of the surface temperature,  $T_w(x) = T_\infty + f_1(x)$ , and, (2) a specified variation of the surface heat flux,  $q_w = f_2(x)$ .  $f_1(x)$  or  $f_2(x)$  can be any arbitrary function representing a differentially heated surface. The power law variations (e.g.  $T_w(x) - T_\infty = ax^n$  and  $q_w = bx^m$ ) used in Refs. [9,14] can be treated as special cases of  $f_1(x)$  or  $f_2(x)$ . The analysis is presented here for the upward surface of the inclined plane (Fig. 1) and for Grashof number values for which the flow remains laminar. For isothermal horizontal surfaces the transition to turbulence commences at  $Gr_x \sim 10^6$ , while the transition starts at  $Gr_x \sim 10^9$  for isothermal vertical surfaces [28,29]. Numerical illustrations are presented in this paper for the range of Grashof number  $10^3 \leq Gr \leq 10^7$ . The limits are not sacrosanct but approximately chosen; the lower limit arises from the requirement that boundary layer type convective flow occurs at a large Grashof number and the upper limit for a laminar theory is set by transition to turbulence.

The fluid properties are assumed to be constant except for the density in the buoyancy term. With this assumption, applying the Boussinesq approximation and neglecting the viscous dissipation in the energy equation, the governing equations for the natural convective boundary layer flow are given by Refs. [1,23–25]:

$$\frac{\partial u}{\partial x} + \frac{\partial v}{\partial y} = 0 \tag{1}$$

$$u \frac{\partial u}{\partial x} + v \frac{\partial u}{\partial y} = -\frac{1}{\rho} \frac{\partial p}{\partial x} + g\beta \sin \gamma (T - T_\infty) + \nu \frac{\partial^2 u}{\partial y^2} \tag{2}$$

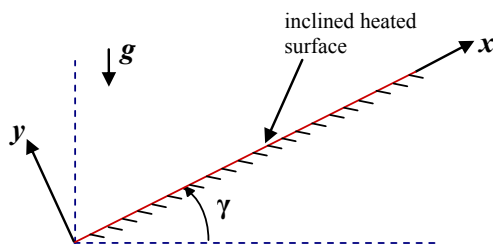


Fig. 1. Physical model and coordinate system.

$$0 = -\frac{1}{\rho} \frac{\partial p}{\partial y} + g\beta \cos \gamma (T - T_\infty) \tag{3}$$

$$u \frac{\partial T}{\partial x} + v \frac{\partial T}{\partial y} = \alpha \frac{\partial^2 T}{\partial y^2} \tag{4}$$

The boundary conditions are

$$\text{At } y = 0, \quad u = 0, \quad v = 0, \quad T_w(x) = T_\infty + f_1(x) \text{ or } q_w = f_2(x) \tag{5a}$$

$$\text{As } y \rightarrow \infty, \quad u \rightarrow 0, \quad T \rightarrow T_\infty, \quad p \rightarrow p_\infty. \tag{5b}$$

Integral analysis of natural convection routinely assumes that the velocity and thermal boundary layers are of equal thickness [1–6,9]. Accordingly, it is also assumed here that both boundary layers are of thickness  $\delta$ . It is explained in Ref. [9] that unlike in forced convection where  $\delta_v \approx \delta_t$  only for  $Pr \sim 1$ , in natural convection  $\delta_v \approx \delta_t$  for  $Pr \leq 1$ . The physical arguments given in Ref. [9] and the similarity results given in Ref. [14], however, show that  $\delta_v > \delta_t$  even in natural convection when  $Pr \gg 1$ . The justification of using the integral analysis in such cases lies in the finding that the Nusselt number predicted by the integral analysis still happens to match with that obtained by the more rigorous similarity analysis. It turns out that, for fluids with  $Pr \gg 1$ , the gradient of the temperature field at the solid surface, that determines the Nusselt number, is predicted reasonably accurately in spite of the inappropriate assumption of the equality  $\delta_v \approx \delta_t$  in the integral analysis.

The general form for a generic temperature profile of order  $\chi$  is given by ([9], see also Appendix A),

$$\frac{\theta}{\theta_w} = \frac{T - T_\infty}{T_w - T_\infty} = \left(1 - \frac{y}{\delta}\right)^\chi. \tag{6}$$

Equation (6) is a general equation where appropriate expressions for  $\theta_w$  needs to be used depending on the specified boundary conditions, as mentioned below.

$$\text{For specified wall temperature, } \theta_w = f_1(x) \tag{7a}$$

$$\text{For specified surface heat flux, } \theta_w = \frac{1}{\chi} f_2(x) \frac{\delta}{k}. \tag{7b}$$

Substituting the expression in (6) into Equation (3) and partially integrating the  $y$ -momentum equation with respect to  $y$  within the limits  $y = y$  and  $y = \delta$ , yields the following expression for the pressure (noting that  $p|_{y=\delta} = p_\infty$ ) [30],

$$p = p_\infty - \rho g \beta \cos \gamma \theta_w \frac{\delta}{\chi + 1} \left(1 - \frac{y}{\delta}\right)^{\chi+1} \tag{8}$$

Partially differentiating the above expression with respect to  $x$  yields,

$$\frac{\partial p}{\partial x} = -\rho g \beta \cos \gamma \frac{\partial}{\partial x} \left( \theta_w \frac{\delta}{\chi + 1} \left(1 - \frac{y}{\delta}\right)^{\chi+1} \right). \tag{9}$$

The general form of the velocity profile of order  $\lambda$  is given by ([9], see also Appendix A)

$$\frac{u}{u_x} = \frac{y}{\delta} \left(1 - \frac{y}{\delta}\right)^{\lambda-1}, \tag{10}$$

where,

$$u_x = \frac{\delta^2}{2(\lambda - 1)v} g\beta \left[ \frac{\cos \gamma}{(\chi + 1)} \frac{d}{dx} (\delta\theta_w) + \theta_w \sin \gamma \right]. \quad (11)$$

Integrating the  $x$ -momentum equation (Equation (2)) in the boundary layer within the limits  $y = 0$  and  $y = \delta$ , the momentum integral equation becomes

$$\underbrace{\frac{d}{dx} \int_0^\delta u^2 dy}_{\text{inertia}} = \underbrace{-\frac{1}{\rho} \int_0^\delta \frac{\partial p}{\partial x} dy}_{\text{indirect pressure difference}} + \underbrace{g\beta \sin \gamma \int_0^\delta (T - T_\infty) dy}_{\text{direct buoyancy}} - \underbrace{v \frac{\partial u}{\partial y} \Big|_{y=0}}_{\text{viscous}}. \quad (12)$$

A pressure gradient normal to the surface ( $\partial p/\partial y$ ) is developed due to the component of the buoyancy force acting normal to the inclined surface ( $g\beta(T - T_\infty)\cos\gamma$ ) as shown in Equation (3). Schlichting and Gersten [11] explained that a gradient of pressure also develops along the surface (i.e.  $\partial p/\partial x$  exists) because of the presence of increased temperature and reduced density inside the boundary layer. Our mathematical analysis, Equation (9), gives the quantitative measure of this pressure gradient term  $\partial p/\partial x$ . This pressure gradient, producing convective flow parallel to the solid surface, was termed 'induced' or 'indirect pressure gradient' by Schlichting and Gersten [11], and is represented by the first term in the RHS of Equation (12). The second term in the RHS of Equation (12) is the component of buoyancy force acting along the inclined surface. This is a measure of the 'direct buoyancy' causing convective flow along the surface. For a horizontal surface ( $\gamma = 0^\circ$ ), the 'direct buoyancy' vanishes and the convective flow in the horizontal direction is driven by the 'indirect pressure difference' alone. On the other hand, for a vertical surface ( $\gamma = 90^\circ$ ), the 'indirect pressure difference' vanishes and the flow is driven along the surface only by the 'direct buoyancy'. For an inclined surface, both mechanisms are operative.

The integral energy equation is obtained by integrating Equation (4) within the limits  $y = 0$  and  $y = \delta$ , and suitably using the relation given in Equation (1):

$$\frac{d}{dx} \int_0^\delta u(T - T_\infty) dy = -\alpha \frac{\partial T}{\partial y} \Big|_{y=0}. \quad (13)$$

Substituting the expression for  $\partial p/\partial x$  [from Equation (9)] and using the temperature and velocity profile approximations [given in Equations (6) and (10)], the integral Equations (12) and (13) can be transformed into the following generalized equations for the natural convective boundary layer flow over inclined flat plates:

$$\frac{1}{\lambda(4\lambda^2 - 1)} \frac{d}{dx} (u_x^2 \delta) = \frac{g\beta \cos \gamma}{(\chi + 1)(\chi + 2)} \frac{d}{dx} (\theta_w \delta^2) + \frac{g\beta \sin \gamma}{(\chi + 1)} \delta \theta_w - v \frac{u_x}{\delta} \quad (14)$$

$$\frac{1}{(\chi + \lambda)(1 + \chi + \lambda)} \frac{d}{dx} (\theta_w u_x \delta) = \frac{\chi \alpha \theta_w}{\delta}. \quad (15)$$

While deriving Equations (12)–(14) appropriate use of the Leibniz's rule has been made [ $d/dx \int_{k(x)}^{l(x)} f(x, y) dy = \int_{k(x)}^{l(x)} \partial f(x, y)/\partial x dy + f(x, l(x)) dl/dx - f(x, k(x)) dk/dx$ ]. The coefficients  $1/\lambda(4\lambda^2 - 1)$  in Equation (14) and  $1/(\chi + \lambda)(1 + \chi + \lambda)$  in Equation (15) have been obtained by using the properties of beta and gamma functions in the evaluation of the corresponding integrals. One consequence of the assumption  $\delta_n = \delta_t = \delta$  in all integral theories is that, with one less variable, one less equation is required [9].

Usually, the separate equation for  $u_x$ , Equation (11), is discarded. Equations (14) and (15) represent two equations specifying the variation of two unknown variables  $u_x$  and  $\delta$  as functions of  $x$ .

The same set of Equations (14) and (15) are applicable for all angles of inclination from the vertical to the horizontal. Secondly, the equations are valid for any integer values of  $\chi$  and  $\lambda$  specifying the temperature and velocity profiles. Thirdly, the same set of Equations (14) and (15) are valid for generalized surface boundary conditions:  $\theta_w$  is to be calculated by Equation (7a) for specified surface temperature, whereas,  $\theta_w$  is to be calculated by Equation (7b) for specified surface heat flux. One example of variable surface temperature is discussed in Section 3.1.3. Finally, the algebra could be carried out such that the effects of variable profile choices (arbitrary values of  $\chi$  and  $\lambda$ ) and arbitrary specification of surface boundary conditions (contained in the definition of  $\theta_w$  given by Equation (7)) are neatly segregated in the final forms of Equations (14) and (15) given above.

When surface temperature is specified, the local heat transfer coefficient  $h_x$  may be evaluated from  $q_w(x) = -k(\partial T/\partial y)_{y=0} = h_x(T_w - T_\infty)$ . Evaluating  $(\partial T/\partial y)_{y=0}$  from Equation (6) and using the expression for  $(T_w - T_\infty)$  from Equation (7a), one obtains the local Nusselt number:

$$Nu_x = \frac{h_x x}{k} = \chi \frac{x}{\delta}. \quad (16)$$

When the surface heat flux is specified, the local heat transfer coefficient is evaluated from  $h_x = q_w(x)/(T_w - T_\infty)$ . Substituting the value of  $(T_w - T_\infty)$  from Equation (7b), one obtains the same expression for  $Nu_x$  as in Equation (16).

Up to now, we have progressed the mathematical formulation for the general case, generic values of  $\chi$  in Equation (6),  $\lambda$  in Equation (10),  $f_1(x)$  in Equation (7a) and  $f_2(x)$  in Equation (7b) have been carried through the analysis. Equations (14)–(16) are thus their most general forms. For numerical illustrations given below, however, specific values of  $\chi$  and  $\lambda$ , and specific functions for  $f_1(x)$  or  $f_2(x)$  are to be chosen.

We have derived the general governing equations for arbitrary variation in surface temperature or surface heat flux so that the readers may use Equations (14) and (15) as required. However, most of the previous experimental or theoretical results are either for isothermal ( $T_w - T_\infty = \text{constant}$ ) or constant surface heat flux ( $q_w = \text{constant}$ ) cases. Therefore, specific forms of equations are developed below for these two important special cases. An illustration of variable surface temperature is treated in Section 3.1.3.

Now, we turn our attention to the appropriate choice of  $\lambda$  and  $\chi$ . A systematic optimization study for horizontal surfaces [9] demonstrated that the optimal choices are  $\lambda = 4$ ,  $\chi = 2$  for isothermal case and  $\lambda = 3$ ,  $\chi = 2$  for constant-heat-flux case, if one wants to build a uniform mathematical formulation over a range of Prandtl numbers ( $0.01 \leq Pr \leq 100$ ). A similar optimization study for vertical surfaces shown in Appendix B also establishes the same criteria. Therefore, for all numerical illustrations given below, we have adopted this optimal choice, viz.  $\lambda = 4$ ,  $\chi = 2$  for isothermal case and  $\lambda = 3$ ,  $\chi = 2$  for constant-heat-flux case. As far as we know, only reference [9] and the present paper have tried to optimize the velocity and temperature profiles for the integral analysis of natural convection. All other references and textbooks seem to adopt, without questioning, the values  $\lambda = 3$ ,  $\chi = 2$  for all boundary conditions and all Prandtl numbers.

The specific forms of the equations for isothermal and constant heat flux cases are described below. The following non-dimensionalised variables have been used while writing the specific forms of the equations:

$$X = \frac{x}{L}, \quad U_x = \frac{u_x}{v/L}, \quad \Delta = \frac{\delta}{L}, \quad (17)$$

The length scale  $L$  chosen here is a physical length along the plate and more specifically, it is a unit length along the semi-infinite plate. This means that a value of  $X = 1$  refers to a point which is at a distance  $L$  downstream of the leading edge. For an isothermal surface,  $L$  is related to the adopted value of Grashof number through the equation  $Gr_L = \frac{g\beta(T_w - T_\infty)L^3}{\nu^2}$ . The natural convection mechanism develops a much shorter length scale perpendicular to the solid surface. The similarity analysis for isothermal horizontal surfaces [14], for example, shows that this new length scale  $\delta \sim L(Gr_L)^{-1/5}$ . In an integral theory, however, an explicit measure of  $\delta$  is not required for deducing the non-dimensional velocity and temperature profiles.

For an isothermal surface ( $T_w - T_\infty = \text{constant}$ ), Equations (14) and (15) can be expressed in the following non-dimensional explicit form, with  $\lambda = 4, \chi = 2$ :

$$\begin{aligned} \text{Term I: Inertia} \quad \text{Term II: Indirect pressure difference} \\ \frac{1}{252} \frac{d}{dX} (U_x^2 \Delta) = \frac{Gr_L \cos \gamma}{12} \frac{d}{dX} (\Delta^2) \\ + \text{Term III: Direct buoyancy} \quad \text{Term IV: Viscous} \\ + \frac{Gr_L \sin \gamma}{3} \Delta - \frac{U_x}{\Delta} \end{aligned} \quad (18)$$

$$\frac{1}{42} \frac{d}{dX} (U_x \Delta) = \frac{2}{Pr \Delta} \quad (19)$$

The Grashof number appearing in Equation (18) is calculated from:

$$Gr_L = \frac{g\beta(T_w - T_\infty)L^3}{\nu^2} \quad (20)$$

Similarly, for a constant-heat-flux surface ( $q_w = \text{constant}$ ), Equations (14) and (15) can be expressed in the following non-dimensional explicit form, with  $\lambda = 3, \chi = 2$ :

$$\begin{aligned} \text{Term I: Inertia} \quad \text{Term II: Indirect pressure difference} \\ \frac{1}{105} \frac{d}{dX} (U_x^2 \Delta) = \frac{Gr_L^* \cos \gamma}{24} \frac{d}{dX} (\Delta^3) \\ + \text{Term III: Direct buoyancy} \quad \text{Term IV: Viscous} \\ + \frac{Gr_L^* \sin \gamma}{6} \Delta^2 - \frac{U_x}{\Delta} \end{aligned} \quad (21)$$

$$\frac{1}{30} \frac{d}{dX} (U_x \Delta^2) = \frac{2}{Pr} \quad (22)$$

The modified Grashof number appearing in Equation (21) is calculated from:

$$Gr_L^* = \frac{g\beta q_w L^4}{k\nu^2} \quad (23)$$

The equation set (18) and (19) or the equation set (21) and (22) have been numerically integrated to obtain the corresponding results presented in this paper. We have attributed a physical meaning to each term of Equations (18) and (21) because one objective of the present paper is to understand the mechanisms of natural convection as the inclination of the surface is changed. This direct physical interpretation of the terms in the simple integral theory would be difficult to achieve if the Navier-Stokes equations were solved by CFD instead. The other advantage of the present method is that solving a set of ordinary differential equations is

**Table 1**  
Comparison of values of  $Nu_x/Gr_x^{1/5}$  obtained by the present integral method with previously published results for isothermal horizontal surfaces.

$Pr$	Integral analysis (present study, $\lambda = 4$ )	Similarity analysis by Samanta and Guha [14]	Numerical solution by Yu and Lin [23]	Numerical solution by Pera and Gebhart [22]
0.01	0.0804	0.0876	0.0708	–
1	0.4024	0.3895	0.3897	0.3940
100	1.0875	1.0896	1.1224	–

much easier (with the accuracy in predicted Nusselt number being demonstrated in Section 3) than solving coupled, non-linear partial differential equations in full-blown CFD methods which would require overcoming numerical instability problems and considerably greater computational time.

It is well known that boundary layer equations have singularity at the leading edge. The integration of the equation set (18) and (19) or the equation set (21) and (22) cannot be started at  $X = 0$ . This problem is overcome by starting the integration at a very small value of  $X$  ( $X = \epsilon$ ), where the initial values of  $U_x$  and  $\Delta$  are determined from the corresponding solutions for a horizontal plate given in Ref. [9]. Several exploratory solutions revealed that this method of initialization of the integration process is robust (works for all inclination angles) and, after a few steps of numerical integration, the value of the Nusselt number obtained at large  $X$  becomes independent of the initial condition.

### 3. Results and discussion

A comparison of the values of the local Nusselt number obtained from the present integral analysis with those given by similarity analysis (for both limiting cases i.e. horizontal and vertical surfaces) and numerical solution of non-similar boundary layer equations shows that the present theory predicts the results accurately and in some cases gives results which agree with the similarity solution even better than other numerical solutions.

Table 1 shows a comparison of the local Nusselt number values for natural convection on isothermal horizontal surfaces, over a wide range of Prandtl numbers, given by similarity analysis [14], numerical solutions [22,23] and the present analysis. For very low (0.01) and very high (100) Prandtl numbers, the values of  $Nu_x$  given by the present analysis are in excellent agreement with similarity

**Table 2**  
Comparison of values of  $Nu_x/Gr_x^{1/4}$  obtained by the present integral method with previously published results for isothermal vertical surfaces.

$Pr$	Integral analysis (present study, $\lambda = 4$ )	Similarity analysis by Burmeister [1]	Similarity analysis by Ostrach [31]	Numerical solution by Yu and Lin [23]
0.01	0.0539	0.0570	–	0.05699
1	0.4183	0.4010	0.4110	0.4004
100	1.4751	1.5495	–	1.5501

**Table 3**  
Comparison of values of  $Nu_x/Gr_x^{*1/6}$  obtained by the present integral method with previously published results for constant heat flux horizontal surfaces.

$Pr$	Integral analysis (present study, $\lambda = 3$ )	Similarity analysis by Samanta and Guha [14]	Numerical correlation by Chen et al. [25]	Numerical solution by Lin et al. [24]
0.01	0.1403	0.1690	–	0.1326
0.7	0.5076	0.5216	0.5203	0.5011
100	1.2810	1.3200	–	1.3261

**Table 4**  
Comparison of values of  $Nu_x/Gr_x^{1/5}$  obtained by the present integral method with previously published results for constant heat flux vertical surfaces.

Pr	Integral analysis (present study, $\lambda = 3$ )	Similarity analysis by Sparrow and Gregg [7]	Numerical solution by Lin et al. [24]
0.1	0.2506	0.2635	0.2635
1	0.5479	0.5339	0.5335
100	1.5455	1.5565	1.5562

solution, and the simple integral analysis is found to give better results than the numerical solution of the non-similar equations [23]. Even for  $Pr = 1$ , the value of  $Nu_x$  deviates from that of similarity analysis by only 3.3%.

In Table 2, the values of the local Nusselt number for natural convection on isothermal vertical surfaces obtained from the present integral analysis are compared with those given by similarity analysis [1,31] and numerical solutions [23]. The results of the present analysis agree reasonably with the results of similarity analysis and other numerical solutions.

Table 3 shows values of the local Nusselt number for natural convection on constant-heat-flux horizontal surfaces obtained from the present integral analysis and those given by similarity analysis [14] and the numerical solution of non-similar boundary layer equations [24,25]. The results of the present analysis agree reasonably with the results of similarity analysis and the other numerical solutions.

In Table 4, the values of the local Nusselt number for natural convection on constant-heat-flux vertical surfaces obtained from the present integral analysis are compared with those given by similarity analysis [7] and numerical solution [24]. The results of the present simple theory agree reasonably with the results of similarity analysis and the other, more elaborate, numerical solutions.

3.1. Comparison of present predictions with previous computational and experimental results for inclined surfaces

Most of the previous studies pertaining to natural convection on inclined surfaces have considered the isothermal and constant heat flux cases. While Sections 3.1.1 and 3.1.2 investigate the predictions of the present integral analysis for the isothermal and constant heat flux cases, Section 3.1.3 describes the natural convective flow over an inclined surface with variable surface temperature.

Usually previous computational or experimental results are

presented in the form of Nusselt number versus Grashof number (or Rayleigh number), with the inclination angle as a parameter. We have, however, used the inclination angle as the abscissa whenever possible. We believe this new representation of the results brings out more powerfully the role of inclination angle in determining the heat transfer rate as well as the mechanism of natural convection.

3.1.1. Results for the isothermal inclined surface

Fig. 2 shows the variation of the local Nusselt number  $Nu_x$  with the angle of inclination  $\gamma$  of the surface, for the isothermal case at  $Pr = 0.7$ . As  $\gamma$  increases,  $Nu_x$  is found to increase with the lowest  $Nu_x$  occurring for the horizontal surface and the highest  $Nu_x$  occurring for the vertical surface. However, the rate of increase of  $Nu_x$  is found to decrease as  $\gamma$  increases. In Fig. 2, we have superposed the numerical solutions of Yu and Lin [23] and Chen et al. [25], and the experimental data of Rich and Burbank [20] which exist in the range  $50^\circ \leq \gamma \leq 90^\circ$ . The experiments were conducted with air and hence  $Pr = 0.7$  is assumed in all three theoretical results shown in Fig. 2. Similarly,  $4.286 \times 10^6$  is the minimum Grashof number at which the experimental data of Rich and Burbank exist; therefore all theoretical calculations are shown at this Grashof number. Chen et al. [25] gave two correlations for two ranges of inclination angle, which are based on numerical computations at two different Prandtl numbers. Their results, as Fig. 2 shows, unfortunately contain a discontinuous jump in the value of the Nusselt number at the boundary of the two ranges of inclination angle (at  $\gamma = 15^\circ$ ), the magnitude of the jump increasing as either the Grashof number or the Prandtl number or both decreases (please see the next two figures to appreciate this aspect). It is hard to imagine a physical reason why such jumps would exist in reality. The results of the present integral analysis match reasonably with the numerical solutions of Yu and Lin [23] and Chen et al. [25] in the range  $\gamma \leq 15^\circ$ , though they deviate to some extent for  $\gamma > 15^\circ$ . However, in the range  $50^\circ \leq \gamma \leq 90^\circ$  for which experimental results of Rich and Burbank [20] exist, the present integral predictions for the Nusselt number are closer to the experimental values than the previous, more elaborate, numerical solutions. It is difficult to extract experimental data directly from the graphs given in the paper of Rich and Burbank [20] or to discern the exact variation of Nusselt number with inclination angle. In plotting the experimental results in Fig. 2, we have therefore used the experimental correlation proposed by Rich and Burbank, which is the same as Eckert's relation except that  $g$  is substituted by  $g \sin \gamma$ . For the limiting cases, the present analysis matches well with the specific value of  $Nu_x$  for

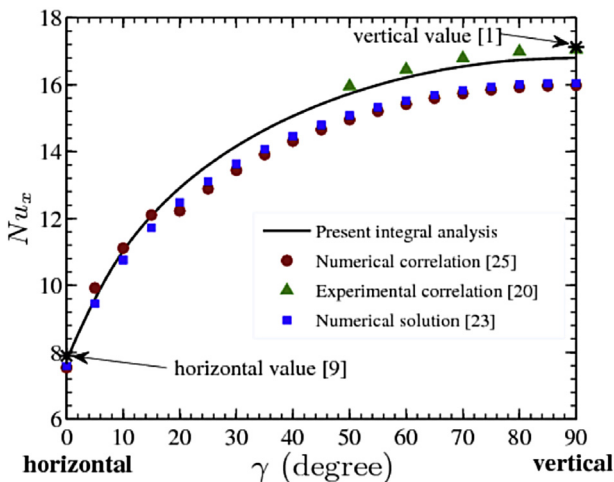


Fig. 2. Local Nusselt number versus inclination angle for an isothermal surface at  $Gr_x = 4.286 \times 10^6$ ,  $Pr = 0.7$  and  $X = 1$ : assessment of the present integral analysis.

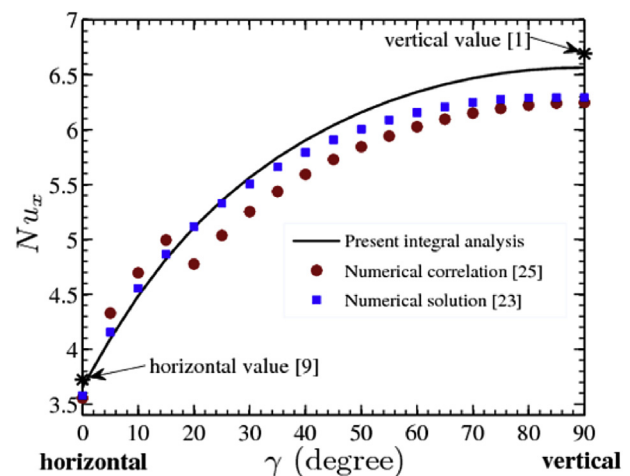


Fig. 3. Local Nusselt number versus inclination angle for an isothermal surface at  $Gr_x = 10^5$ ,  $Pr = 0.7$  and  $X = 1$ : assessment of the present integral analysis.

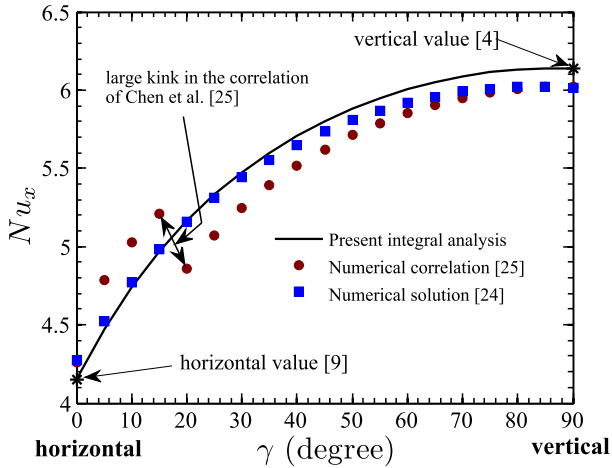


Fig. 4. Local Nusselt number versus inclination angle for a constant heat flux surface at  $Gr_x^* = 3 \times 10^5$ ,  $Pr = 0.7$  and  $X = 1$ : assessment of the present integral analysis.

vertical surfaces given by Burmeister [1] and that for horizontal surfaces given by Guha and Samanta [9].

Fig. 3 also shows the variation of the local Nusselt number with inclination angle at  $Pr = 0.7$ , but at a lower value of  $Gr_x^*$  as compared to that in Fig. 2. It is observed that the correlations of Chen et al. [25] contain a discontinuous jump (of a greater magnitude than that in Fig. 2) in the value of the Nusselt number at  $\gamma = 15^\circ$ . The magnitude of the apparently non-physical jump is greater in Fig. 3 as compared to that in Fig. 2 owing to the smaller value of Grashof number assumed here. The results of the present simple theory match reasonably with the numerical solution of Yu and Lin [23] in the range  $\gamma \leq 35^\circ$ . For the limiting cases, the present theory matches well with the specific values of  $Nu_x$  given by Burmeister [1] for vertical surfaces and Guha and Samanta [9] for horizontal surfaces.

3.1.2. Results for the constant-heat-flux inclined surface

Fig. 4 shows the variation of the local Nusselt number  $Nu_x$  with the angle of inclination  $\gamma$  of the surface, for the constant surface heat flux case at  $Pr = 0.7$ . As for the isothermal case,  $Nu_x$  is found to increase with increasing  $\gamma$ , with the rate of increase of  $Nu_x$  decreasing with increasing  $\gamma$ . Fig. 4 also shows that the correlations of Chen et al. [25] contain a discontinuous, apparently non-

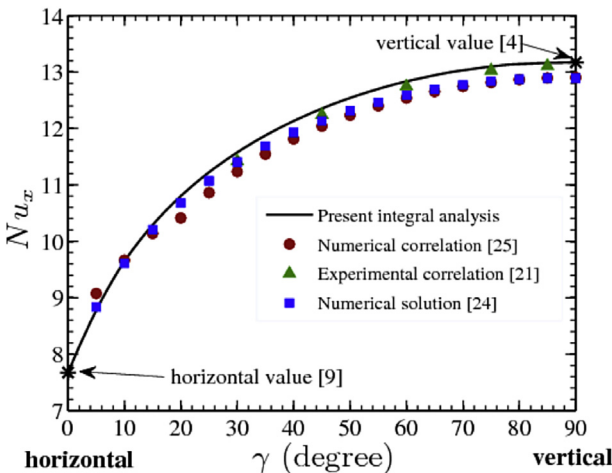


Fig. 5. Local Nusselt number versus inclination angle for a constant heat flux surface at  $Gr_x^* = 0.71 \times 10^6$ ,  $Pr = 7$  and  $X = 1$ : assessment of the present integral analysis.

Table 5

Comparison of the local Nusselt number  $Nu_x$  obtained by the present integral method with the numerical results of Chen et al. [25] for  $\gamma = 15^\circ$ ,  $Pr = 0.7$ ,  $X = 1$  and  $T_w - T_\infty = ax$ .

$Gr_x^*$	Present integral solution	Solution of Chen et al. [25]
$10^3$	2.34	2.35
$10^4$	3.93	4.02
$10^5$	6.69	6.89
$10^6$	11.58	11.80

physical, jump in the value of the Nusselt number at  $\gamma = 15^\circ$  (as mentioned previously, the magnitude of jump in Fig. 4 is greater than that in Fig. 2 because the assumed Grashof number is lower here). The results of the present integral analysis match reasonably with the numerical solutions of Lin et al. [24] in the range  $\gamma \leq 50^\circ$ , though they deviate slightly for  $\gamma > 50^\circ$ . For the limiting cases, the present theory matches well with the specific value of  $Nu_x$  for vertical surfaces given by Sparrow [4] and that for horizontal surfaces given by Guha and Samanta [9].

Fig. 5 shows the variation of the local Nusselt number  $Nu_x$  with the angle of inclination  $\gamma$  of the surface, for the constant surface heat flux case at  $Pr = 7$ . As for the isothermal case,  $Nu_x$  is found to increase with increasing  $\gamma$ , with the rate of increase of  $Nu_x$  decreasing with increasing  $\gamma$ . In Fig. 5, we have superposed the numerical solutions of Lin et al. [24] and Chen et al. [25], and, the experimental data of Vliet [21] which exist in the range  $30^\circ \leq \gamma \leq 85^\circ$ . The experiments were conducted with water and hence  $Pr = 7$  is assumed in all three theoretical results shown in Fig. 5. Similarly,  $0.71 \times 10^6$  is the minimum Grashof number at which the experimental data of Vliet exist; therefore all theoretical calculations are shown at this Grashof number. It is difficult to extract experimental data directly from the graphs given in the paper of Vliet [21], or to discern the exact variation of Nusselt number with inclination angle. The axes in the plots given in Ref. [21] are logarithmic and hence small errors in measurement are magnified in the plots presented in the present paper which have linear axes. Since the main focus of the present paper is the effect of inclination angle on the Nusselt number, we have presented all the Nusselt number plots with inclination angle  $\gamma$  as the abscissa while maintaining the value of  $Gr_x^*$  constant. However, the plots shown in Ref. [21] are variations of the local Nusselt number with modified Rayleigh number, and almost no two inclination angle data were found for the same value of  $Gr_x^*$ . So, plotting the experimental results directly in the  $Nu_x$  vs  $\gamma$  graphs would require multiple graphs, one for each value of  $Gr_x^*$  and therefore, we have used the correlations developed by Vliet instead. A comparative study of the curves in Figs. 2–5 demonstrates that the present simple theory captures the essential physics and does well in predicting the Nusselt number as a function of the Grashof number, Prandtl number and inclination angle (for all inclination angles from the horizontal to the vertical configuration).

3.1.3. Results for inclined surface with variable surface temperature

All illustrations in Sections 3.1.1 and 3.1.2 are for constant surface temperature and constant surface heat flux cases respectively. Here, we investigate the case of a surface whose temperature increases linearly with distance from the leading edge (i.e.,  $T_w - T_\infty = ax$ ), as an example of the suitability of the present formulation for the case of variable surface temperature. The integral momentum and energy equations describing the natural convective flow over an inclined surface for the particular variation of surface temperature ( $T_w - T_\infty = ax$ ) are obtained by substituting  $\theta_w$  by  $ax$  in Equations (14) and (15), and are listed below:

$$\frac{1}{252} \frac{d}{dX} (U_x^2 \Delta) = \frac{Gr_L \cos \gamma}{12} \frac{d}{dX} (X \Delta^2) + \frac{Gr_L \sin \gamma}{3} X \Delta - \frac{U_x}{\Delta} \tag{24}$$

$$\frac{1}{42} \frac{d}{dX} (X U_x \Delta) = \frac{2X}{Pr \Delta} \tag{25}$$

For this case, the Grashof number is defined by:

$$Gr_L = \frac{g \beta a L^4}{\nu^2} \tag{26}$$

$\lambda = 4$  and  $\chi = 2$  have been used while deriving Equations (24) and (25) from Equations (14) and (15).

The values of the local Nusselt number  $Nu_x$  obtained by solving Equations (24) and (25) for  $\gamma = 15^\circ$ ,  $Pr = 0.7$  and different values of the Grashof number are shown in Table 5 alongside the numerical solution given by Chen et al. [25]. It is observed that the predictions of the present analysis compare reasonably with the numerical solutions given in Ref. [25].

Unfortunately, no experimental data is available for inclined surfaces with arbitrary variation in surface temperature or heat flux. Hence, experimental validation of this versatility of the present formulation is not possible at the time. In the following discussion, we therefore return to the specific cases of isothermal and constant-heat-flux inclined surfaces, since the main focus of the present paper is to demonstrate the ability of the present integral analysis to capture the physics of natural convection as the inclination angle of the solid surface is varied from the vertical to horizontal.

### 3.2. Analytical formulae for limiting cases of inclination angle

There are two limiting cases, viz. horizontal ( $\gamma = 0^\circ$ ) and vertical ( $\gamma = 90^\circ$ ). Similarity solutions exist for both limiting cases. One important implication is that the integral theories lead to closed-form analytical solutions for the Nusselt number for both limiting cases [1,9].

One characteristic of integral analyses is that the computed Nusselt number depends on the choice of velocity and temperature profiles. It was demonstrated in Ref. [9] that, for natural convection on an isothermal horizontal surface,  $\lambda = 4$  and  $\chi = 2$  are the optimal choices respectively for the velocity and temperature profiles, if one wants to build a generic integral analysis over a range of Prandtl numbers ( $0.01 \leq Pr \leq 100$ ). Similarly, it was demonstrated in Ref. [9] that, for natural convection on a horizontal surface subjected to constant heat flux,  $\lambda = 3$  and  $\chi = 2$  are the optimal choices if one wants to build a generic integral analysis over a range of Prandtl numbers ( $0.01 \leq Pr \leq 100$ ). In a recent unpublished work [32], the same analytical procedure, described in Ref. [9], was applied to the case of vertical surfaces and it was found that the above conclusions regarding the optimum choices for velocity and temperature profiles also hold here (a short summary is given in Appendix B for ready reference). We believe this optimization study for the vertical surface is new and the results (Table B1 of Appendix B) are new, since all previous integral studies for vertical surfaces (e.g given in Refs. [1–4]) use, to the best of our knowledge,  $\lambda = 3$  and  $\chi = 2$ . We summarize the final forms of the analytical formulae for Nusselt number below, as they will be useful in the following discussion and also as a general resource for future researchers.

For isothermal vertical surface with  $\lambda = 4$ ,  $\chi = 2$ , the Nusselt number ( $Nu_{x,vt}$ ) is given by (Appendix B):

$$Nu_{x,vt} = 0.467 \left( \frac{Gr_x Pr^2}{\frac{5}{9} + Pr} \right)^{1/4} \tag{27}$$

For constant-heat-flux vertical surface with  $\lambda = 3$ ,  $\chi = 2$ , the Nusselt number ( $Nu_{x,vq}$ ) is given by (Appendix B):

$$Nu_{x,vq} = 0.616 \left( \frac{Gr_x^* Pr^2}{\frac{4}{5} + Pr} \right)^{1/5} \tag{28}$$

For isothermal horizontal surface with  $\lambda = 4$ ,  $\chi = 2$ , the Nusselt number ( $Nu_{x,ht}$ ) is given by [9]:

$$Nu_{x,ht} = 0.433 \left( \frac{Gr_x Pr^2}{\frac{4}{9} + Pr} \right)^{1/5} \tag{29}$$

For constant-heat-flux horizontal surface with  $\lambda = 3$ ,  $\chi = 2$ , the Nusselt number ( $Nu_{x,hq}$ ) is given by [9]:

$$Nu_{x,hq} = 0.595 \left( \frac{Gr_x^* Pr^2}{\frac{7}{4} + Pr} \right)^{1/6} \tag{30}$$

For several physical and mathematical insight on the generic integral analysis, including a discussion on the relative thicknesses of the velocity and temperature boundary layers in natural convection and the role of Prandtl number in determining their relative magnitudes (which is fundamentally different from the well-known role of Prandtl number in forced convection), the reader is referred to [9].

Due to the nature of the coupling of the velocity and temperature fields in natural convection, the velocity boundary layer cannot be thinner than the thermal boundary layer. Thus for fluids with  $Pr \leq 1$ , the two boundary layer thicknesses are of comparable magnitude. For high  $Pr$  fluids ( $Pr \gg 1$ ), the effects of viscosity are transmitted to a considerable distance normal to the surface and hence, the velocity boundary layer is thicker than the thermal boundary layer. Inside the thermal boundary layer ( $y \leq \delta_t$ ), the buoyancy force is balanced by the viscous force. Beyond  $y = \delta_t$ , the motion of the fluid is controlled by inertia and viscous force [9].

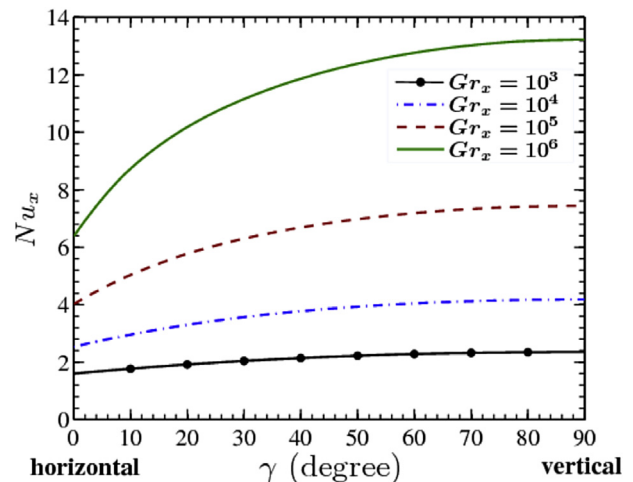


Fig. 6. Local Nusselt number versus inclination angle for an isothermal surface at  $Pr = 1$  and  $X = 1$ .

3.3. Exploration for possible scaling laws

The figures that have been presented so far in this paper show the variation of the local Nusselt number with the inclination angle for specific values of  $Gr_x$  and  $Pr$ . In order to avoid multiplicity of graphs and at the same time provide information on a range of values of the parameters  $Gr_x$  and  $Pr$ , it would be great if one can scale the local Nusselt number in such a manner that the multiple curves collapse to a single curve (for a particular surface boundary condition). In this section, we explore various possibilities of scaling and determine the success of each method over a range of important parameters.

Fig. 6 shows the variation of  $Nu_x$  with  $\gamma$  for  $Pr = 1$  at different values of the Grashof number. As  $Gr_x$  increases the value of  $Nu_x$  increases, and the rate of this increase also increases with increasing  $Gr_x$ . However, this figure is unable to provide precise quantitative information about  $Nu_x$  at values of  $Gr_x$  other than those mentioned in the figure. An appropriate scaling can therefore lead to concise yet comprehensive representation of data.

Equation (27) shows that the Nusselt number for isothermal vertical surfaces is scaled by the one-fourth power of the Grashof number. However, Equation (29) shows that, for isothermal horizontal surfaces, the one-fifth power of the Grashof number is the scaling factor. It is therefore anticipated that there may not be a universal scaling factor at all inclination angles, but it would still be interesting to find what is the scaling factor that would cover the maximum range of the involved parameters. This would give insight on physical mechanisms of natural convection operative at various angles of inclination and explain the rationale of the adopted ranges of parameters for correlations available in the literature. The following discussion relates to isothermal surfaces. Similar conclusions (this time taking help of Equations (28) and (30)) were found to apply for surfaces with constant heat flux but are not reported here for brevity.

Taking inspiration from the result for the vertical surface (Equation (27)), one-fourth power of the local Grashof number is first considered as the scaling factor. Fig. 7 shows the local Nusselt number scaled by  $Gr_x^{1/4}$ , at  $Pr = 1$ . For the range of inclination  $42^\circ \leq \gamma \leq 90^\circ$ , the curves for the different values of  $Gr_x$  collapse to a single curve. This shows that the mechanism of natural convection on a vertical surface dominates in this range of inclination while the horizontal mechanism comes into play in the range  $\gamma < 42^\circ$ . Extensive computations show that the range of inclination angles for which the vertical mechanism dominates is increased as the

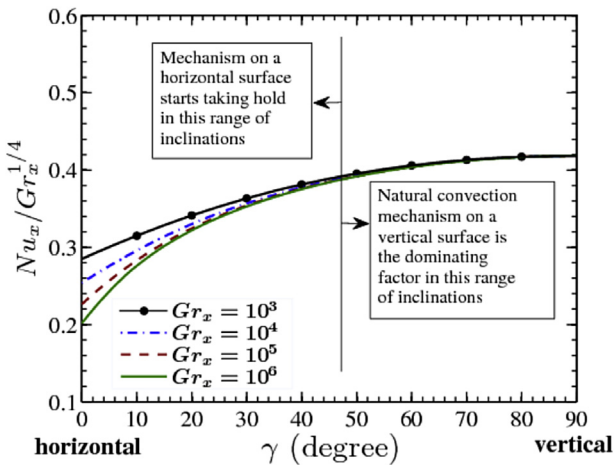


Fig. 7. Reduced local Nusselt number versus inclination angle for an isothermal surface at  $Pr = 1$  and  $X = 1$ .

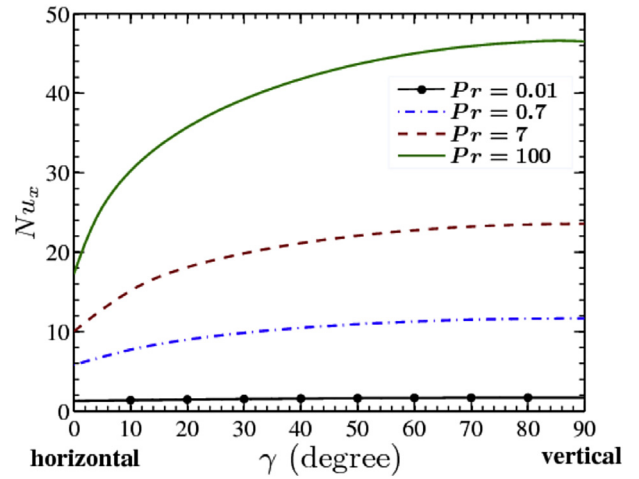


Fig. 8. Local Nusselt number versus inclination angle for an isothermal surface at  $Gr_x = 10^6$  and  $X = 1$ .

Prandtl number increases. For  $Pr = 100$ , the curves for different  $Gr_x$  collapse to a single curve in the range  $15^\circ \leq \gamma \leq 90^\circ$ . However, for  $Pr = 0.01$ , this range decreases to  $83^\circ \leq \gamma \leq 90^\circ$ . It was also found in the course of the present study that the scaling of  $Nu_x$  with  $Gr_x^{1/5}$  does not result in a single curve for different  $Gr_x$  values at inclinations other than the horizontal.

Fig. 8 shows the variation of  $Nu_x$  with inclination angle on an isothermal surface for different values of the Prandtl number, Grashof number being kept at a fixed value. As  $Pr$  increases,  $Nu_x$  increases for all inclinations of the isothermal surface. However, this figure is unable to provide precise quantitative information about  $Nu_x$  at values of  $Pr$  other than those mentioned in the figure. Therefore, the Nusselt number needs to be scaled with the Prandtl number (in addition to the scaling with the Grashof number, which has been illustrated in Fig. 7) in such a way that the four curves would tend to collapse to a single curve. In that way,  $Nu_x$  can be determined for any value of  $Gr_x$  and  $Pr$  for different inclination angles from that single curve.

The local Nusselt number on an isothermal vertical surface ( $Nu_{x,v}$ ) is given by Equation (27). It was found in Fig. 7 that the natural convection mechanism on a vertical surface dominates over a range of inclination angles while there is no such dominance of the horizontal mechanism. Hence, it is proposed that  $Nu_x$  be scaled with  $Nu_{x,v}$ .

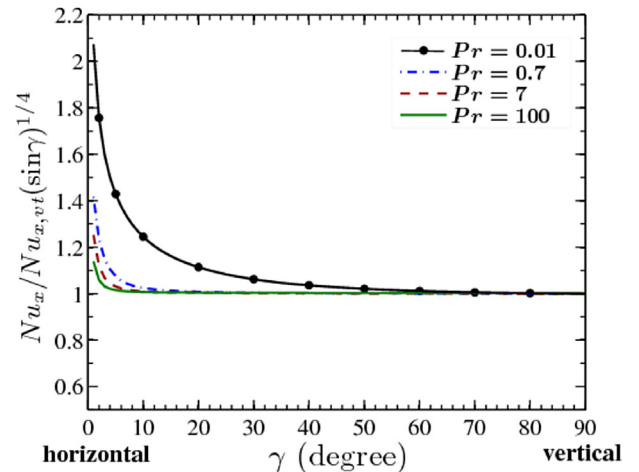


Fig. 9. Reduced local Nusselt number versus inclination angle for an isothermal surface at  $Gr_x = 10^6$  and  $X = 1$ .

A plot of  $Nu_x/Nu_{x,vt}$  with the inclination angle  $\gamma$  shows that the curves for  $Pr = 0.7$ ,  $Pr = 7$  and  $Pr = 100$  collapse to a single curve in the range  $30^\circ \leq \gamma \leq 90^\circ$ , while the curve for  $Pr = 0.01$  deviates from the group for  $\gamma < 80^\circ$ . However, it is not possible to ascertain the range of inclination angle for which the vertical mechanism of natural convection dominates for various values of  $Pr$ . In order to address this issue, it is recognized that, for an inclined surface, only a component of gravity acts along the surface. Thus, if the convection mechanism on a vertical surface is the dominating factor at other inclinations also, then  $g$  in the Grashof number can be replaced by  $g\sin\gamma$ . Thus a new scaling factor  $Nu_{x,vt}(\sin\gamma)^{1/4}$  was tried and the results are shown in Fig. 9.

Owing to the division by  $\sin\gamma$ , the scaled Nusselt number is undefined at  $\gamma = 0^\circ$ , and the curves in Fig. 9 are shown for  $1^\circ \leq \gamma \leq 90^\circ$ . Although the curves in Fig. 9 show upward trend near  $\gamma = 0^\circ$ , it should be remembered that the actual values of  $Nu_x$  for a horizontal surface is always smaller than that for a vertical surface for given values of  $Gr_x$  and  $Pr$  (see Figs. 6 and 8). A horizontal line in Fig. 9 with ordinate value equal to unity signifies that the mechanism for natural convection on a vertical surface drives the convective flow. For  $Pr = 0.01$ , the curve deviates from unity at around  $\gamma = 60^\circ$ . However for  $Pr = 0.7$ ,  $Pr = 7$  and  $Pr = 100$ , the curves remain parallel to the  $\gamma$  axis at an ordinate value of unity in the range  $15^\circ \leq \gamma \leq 90^\circ$ . This establishes the rationale for why previous studies (e.g. Chen et al. [25]) had to use two separate correlations for the ranges  $0^\circ \leq \gamma \leq 15^\circ$  and  $15^\circ \leq \gamma \leq 90^\circ$ . Our study also shows that such a division of range in inclination angle is valid at moderate to high Prandtl numbers and would break down when the Prandtl number is low. This has not been identified in the work of Chen et al. [25] since they performed the calculations only at two Prandtl numbers ( $Pr = 0.7$  and  $Pr = 7$ ).

There is a second subtle point which depends on the value of  $Gr_x$ . Fig. 9 is drawn for  $Gr_x = 10^6$ . When similar calculations are repeated at other values of  $Gr_x$ , it is found that the curves for  $Pr = 0.7$ ,  $Pr = 7$  and  $Pr = 100$  start deviating from each other at different values of  $\gamma$  (i.e. the angle  $15^\circ$ , mentioned in the previous paragraph, is not a sacrosanct value). The general trend is that as  $Gr_x$  is decreased, the demarcating angle increases. This trend can also be appreciated from an inspection of Fig. 7.

It is worth mentioning here that the proposed scaling laws account for the variation of Prandtl number through the vertical surface Nusselt number  $Nu_{x,vt}$  which is a function of  $Pr$  (see Equation (27)). Therefore, the scaling laws have been explored for a range of values of  $Gr$  and  $Pr$ .

3.4. Proposed correlations:  $Nu_x = f(Gr_x, Pr, \gamma)$  or  $Nu_x = f(Gr_x^*, Pr, \gamma)$

From a practical, engineering point of view it is useful to formulate a correlation of the form  $Nu_x = f(Gr_x, Pr, \gamma)$  or  $Nu_x = f(Gr_x^*, Pr, \gamma)$ ,  $Gr_x$  being used when surface temperature is specified and  $Gr_x^*$  being used when surface heat flux is specified.

3.4.1. Correlation of Type I

It was proposed by Churchill [33] that the local Nusselt number for mixed convection laminar boundary layer flows can be correlated very well by combining the local Nusselt number for pure forced convection and that for pure natural convection. Taking cue from this and a few other studies [23,24], correlations of the following form are proposed for the local Nusselt number for inclined isothermal surfaces by combining the local Nusselt numbers for the vertical and horizontal orientations:

$$[Nu_{x,t}(Gr_x, Pr, \gamma)]^n = [Nu_{x,ht}(\cos\gamma)^{1/5}]^n + [Nu_{x,vt}(\sin\gamma)^{1/4}]^n \tag{31}$$

In our formulation,  $Nu_{x,ht}$  is given by Equation (29) and  $Nu_{x,vt}$  is given by Equation (27). It is to be noted that the Prandtl number dependence in Equations (29) and (27) is mathematically deduced. The Nusselt number given by Equation (31) correctly reduces to  $Nu_{x,ht}$  at  $\gamma = 0^\circ$  and to  $Nu_{x,vt}$  at  $\gamma = 90^\circ$ . A comparison of the present numerical results and the prediction of Equation (31) shows that  $n = 5$  is a good choice and keeps the prediction of the correlation within  $\pm 2\%$  of the numerical results for the ranges of parameters investigated ( $10^3 \leq Gr_x \leq 10^7$ ,  $0.01 \leq Pr \leq 100$ ,  $0^\circ \leq \gamma \leq 90^\circ$ ).

Similarly, taking cue from previous studies, the following correlation is proposed for surfaces with constant heat flux:

$$[Nu_{x,q}(Gr_x^*, Pr, \gamma)]^n = [Nu_{x,hq}(\cos\gamma)^{1/6}]^n + [Nu_{x,vq}(\sin\gamma)^{1/5}]^n \tag{32}$$

$Nu_{x,hq}$  is given by Equation (30) and  $Nu_{x,vq}$  is given by Equation (28). It is to be noted that the Prandtl number dependence in Equations (30) and (28) is mathematically deduced. The Nusselt number given by Equation (32) correctly reduces to  $Nu_{x,hq}$  at  $\gamma = 0^\circ$  and to  $Nu_{x,vq}$  at  $\gamma = 90^\circ$ . A comparison of the present numerical results and the prediction of Equation (32) shows that  $n = 6$  is a good choice and keeps the prediction of the correlation within  $\pm 1\%$  of the numerical results for the ranges of parameters investigated ( $10^3 \leq Gr_x^* \leq 10^7$ ,  $0.01 \leq Pr \leq 100$ ,  $0^\circ \leq \gamma \leq 90^\circ$ ). However, the form of the above correlations makes it difficult to establish the dominating convection mechanism prevalent for a particular inclination of the surface. Consequently, an attempt is made below to propose correlations which give a direct indication of the dominating convection mechanism.

3.4.2. Correlation of Type II

One can also formulate a different form of correlations (referred to as Type II here), where the cue is taken from Figs. 7 and 9. One advantage of this type of correlation is that direct physical interpretation of the terms is possible and it is easier to relate the correlation to the behaviour observed in Figs. 7 and 9 and similar figures. Fig. 9, for example, clearly shows that, at moderate to high Prandtl number, the actual variation of the Nusselt number is captured well by  $Nu_{x,vt}(\sin\gamma)^{1/4}$  over a large range of inclination angles except when the inclination is close to the horizontal. The range of inclination angles (close to  $\gamma = 0^\circ$ ) over which deviation is observed increases in extent as either the Prandtl number or the Grashof number decreases. In order to capture this behaviour, it is postulated here that the generic form of the correlations of Type II would be:

$$Nu_x = Nu_{x,v}(\sin \gamma)^{n_1} + c Nu_{x,h} \tag{33}$$

where,

$$c = \exp(-\gamma^{n_2}/b) \tag{34}$$

The exponential form for  $c$  is postulated from the features of Fig. 9, explained previously. The exponent  $n_1$  in Equation (33) depends on the surface boundary condition (i.e. whether temperature or heat flux is specified), as we have already found. It is anticipated that  $n_2$  in Equation (34) will also depend on the surface boundary condition, though  $n_2$  may not necessarily be the same as  $n_1$ . It is expected that  $b$  in Equation (34) will be a function of  $Gr_x$  (or  $Gr_x^*$ ) and  $Pr$ , and, it is hoped that  $b$  is not a function of  $\gamma$ . The particular form assumed for  $c$ , through Equation (34), ensures that  $c$  possesses the correct behaviour in two known limits, viz.  $c \rightarrow 1$ , as  $\gamma \rightarrow 0^\circ$ , and,  $c \rightarrow 0$ , as  $\gamma \rightarrow 90^\circ$ .

On the basis of a large number of computations, the following specific forms of Equation (33) are developed for the isothermal and constant-heat-flux cases.

Isothermal case:

$$Nu_x = Nu_{x,vt}(\sin \gamma)^{1/4} + cNu_{x,ht} \tag{35}$$

$$c = \exp\left(-\gamma^{2/5}/b\right) \tag{36}$$

$$b = 2.023\left(Pr^2 Gr_x\right)^{-0.064} \tag{37}$$

$\gamma$  in Equation (36) is to be expressed in degree.  $Nu_{x, vt}$  is given by Equation (27) and  $Nu_{x,ht}$  is given by Equation (29). The Nusselt number given by Equation (35) correctly reduces to  $Nu_{x,ht}$  at  $\gamma = 0^\circ$  and to  $Nu_{x,vt}$  at  $\gamma = 90^\circ$ . A comparison of the present numerical results and the prediction of Equation (35) shows that the maximum error is within  $\pm 3\%$  of the numerical results for the ranges of parameters investigated ( $10^3 \leq Gr_x \leq 10^7$ ,  $0.01 \leq Pr \leq 100$ ,  $0^\circ \leq \gamma \leq 90^\circ$ ). The maximum deviation is found to occur at low Grashof number and high Prandtl number.

Constant-heat-flux case:

$$Nu_x = Nu_{x,vq}(\sin \gamma)^{1/5} + cNu_{x,hq} \tag{38}$$

$$c = \exp\left(-\gamma^{1/3}/b\right) \tag{39}$$

$$b = 1.7219\left(Pr^2 Gr_x^*\right)^{-0.0454} \tag{40}$$

$\gamma$  in Equation (39) is to be expressed in degree.  $Nu_{x,vq}$  is given by Equation (28) and  $Nu_{x,hq}$  is given by Equation (30). The Nusselt number given by Equation (38) correctly reduces to  $Nu_{x,hq}$  at  $\gamma = 0^\circ$  and to  $Nu_{x,vq}$  at  $\gamma = 90^\circ$ . A comparison of the present numerical results and the prediction of Equation (38) shows that the maximum error is within  $\pm 4\%$  of the numerical results for the ranges of parameters investigated ( $10^3 \leq Gr_x^* \leq 10^7$ ,  $0.01 \leq Pr \leq 100$ ,  $0^\circ \leq \gamma \leq 90^\circ$ ). The maximum deviation is found to occur at low Grashof number and low Prandtl number.

It is to be noted that, unlike several empirical formulae available in the literature, Equations 27–30 giving the Grashof number and Prandtl number dependence in the vertical and horizontal limits ( $Nu_{x,vt}$ ,  $Nu_{x,ht}$ ,  $Nu_{x,vq}$ ,  $Nu_{x,hq}$ ) are the results of rigorous mathematical derivation.

### 3.5. Mechanisms of natural convection

The physical mechanism of natural convection on a vertical surface is very different from that over a horizontal surface. For a vertical surface, buoyancy is generated because of the temperature difference between the surface and the fluid. The buoyancy force is parallel to the surface and creates fluid motion along the vertical surface that carries away heat from the surface (when the surface is hotter than the surrounding fluid) or supplies heat to the surface (when the surface is colder than the surrounding fluid). On a horizontal surface, the buoyancy force is perpendicular to the surface. The natural convective motion along the horizontal surface is set up by an indirectly generated pressure difference [11]. The governing Equation (18) derived in this paper beautifully captures this stark difference in the mechanisms of natural convection. For a vertical surface (i.e.  $\gamma = 90^\circ$ ), the Term II in Equation (18), representing the indirect pressure difference, drops out and the sole cause for the generation of natural convection on a vertical surface becomes the Term III, i.e. the direct buoyancy force. For a horizontal surface (i.e.  $\gamma = 0^\circ$ ), on the other hand, the Term III in Equation (18), representing the direct buoyancy force, drops out and the sole cause for

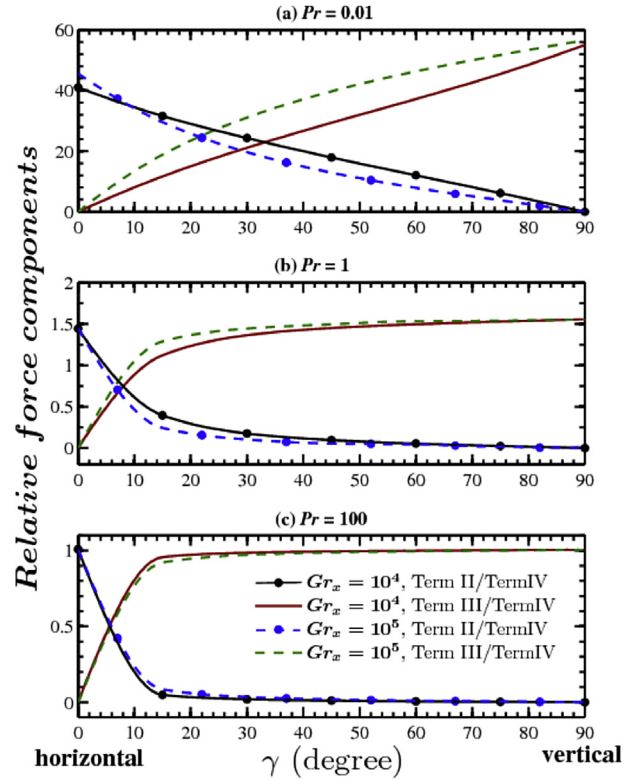


Fig. 10. Dependence of the relative force components for natural convection on inclined isothermal surfaces on the Prandtl number and the Grashof number. Term II, Term III and Term IV represent the forces due to ‘indirect pressure difference’, ‘direct buoyancy’ and ‘viscous effects’ respectively, as shown in Equation (18).

the generation of natural convection on a horizontal surface becomes the Term II, i.e. the indirect pressure difference. For surfaces at intermediate angles, both source terms (i.e. Term II and Term III) are operative, but through a comprehensive analysis we have been able to establish the generic trend in the relative magnitudes of the two source terms as a function of Grashof number, Prandtl number and inclination angle.

Fig. 10 demonstrates the influence of the Prandtl number of the fluid and the inclination angle of the solid surface on the relative importance of the components of forces that set up the natural convective flow, viz. the direct buoyancy force (represented by  $\frac{Gr_L \sin \gamma \Delta}{3}$  in Equation (18)), viscous force (represented by  $\frac{U_x}{\Delta}$  in Equation (18)) and the force due to indirect pressure difference (represented by  $\frac{Gr_L \cos \gamma}{12} \frac{d}{dx} (\Delta^2)$  in Equation (18)). It may be observed that for a given value of the Grashof number and at a given distance from the leading edge, these forces depend on the inclination of the surface  $\gamma$  and the thickness of the boundary layer  $\Delta$ . The value of  $\Delta$  is a function of the Grashof number, distance from the leading edge and the Prandtl number (see Equation (19)). Thus, though the Prandtl number does not appear explicitly in the expressions of the forces, its effect on the relative importance of the forces (which determines the dominating mechanism) is present through the value of  $\Delta$ . As explained previously, when the direct buoyancy force dominates (i.e. it is approximately an order of magnitude greater than its counterpart), the mechanism of natural convection on a vertical surface mainly drives the convective flow. On the other hand, when the force due to the indirect pressure difference dominates, the mechanism of natural convection on a horizontal surface is the main driving force. The viscous force, however, opposes the flow for any surface configuration. Fig. 10a shows that, for  $Pr = 0.01$ , the direct buoyancy force and the force due to the indirect

pressure difference are comparable over almost the entire range of inclination angles except when  $\gamma$  is close to either  $0^\circ$  or  $90^\circ$ , and the vertical mechanism dominates for only near vertical configurations (i.e. when  $\gamma \sim 90^\circ$ ). As a result, the scaling law explored in the previous section (using  $Nu_{x,vt}(\sin\gamma)^{1/4}$  as the scaling factor) works for only a small range of inclination angles close to the vertical configuration. For  $Pr = 1$  and  $Pr = 100$ , according to Fig. 10b and c, the direct buoyancy force dominates over the force due to indirect pressure difference over a greater range of inclination angles. This signifies that the mechanism of natural convection on vertical surfaces drives the convective flow for even inclination angles as low as  $\gamma \sim 40^\circ$ . This establishes the reason for the scaling factor of  $Nu_{x,vt}(\sin\gamma)^{1/4}$  working over a greater range of inclination angles for moderate to high Prandtl numbers (as seen in Fig. 9). The considerably greater magnitudes of the relative force components for  $Pr = 0.01$  (see the  $y$ -axis labels in Fig. 10a, as compared to the  $y$ -axis labels in Fig. 10b and c) may be attributed to the reduced viscosity at low Prandtl numbers.

Fig. 10 also includes the effect of Grashof number on the variation of relative force components; the computations being carried out at two values of Grashof number ( $10^4$  and  $10^5$ ). It is found that the cross-over point (the point at which Term II = Term III, i.e. the direct buoyancy is equal to indirect pressure difference) occurs at a lower value of  $\gamma$  as the Grashof number is increased, i.e. the horizontal convection mechanism loses its relative importance closer to the horizontal orientation as the Grashof number is increased. This shifting of the cross-over point is more pronounced as the Prandtl number decreases.

#### 4. Conclusion

In the present study we have formulated, for the first time, a unified integral theory (with optimized orders of velocity and temperature profiles) for natural convection on an arbitrarily inclined surface, both for specified variation in surface temperature ( $T_w(x) = T_\infty + f_1(x)$ ) and surface heat flux ( $q_w = f_2(x)$ ), such that the Nusselt number matches with results obtained from the similarity analysis in the limiting cases of vertical and horizontal surfaces. The predictions of the present formulation also agree well with previous computational and experimental results at intermediate angles of inclination between the vertical and the horizontal.  $f_1(x)$  or  $f_2(x)$  can be any arbitrary function, including power law variation, and represents a differentially heated surface. The strength of the present theory lies in its simplicity while its predictions agree with more complex computations and experiments. The other strength of the present theory lies in its unified nature so that the same set of Equations [(14) and (15)] are applicable for any value of the inclination angle (between the vertical and horizontal), Grashof number and Prandtl number, and, can accommodate arbitrarily complex surface boundary conditions. Another important feature of the present integral theory is that Equations (14) and (15) can accommodate arbitrary orders of polynomials ( $\lambda$  and  $\chi$ ) representing the velocity and temperature profiles, and optimum values for  $\lambda$  and  $\chi$  have been systematically determined for various boundary conditions (i.e.  $\lambda = 4$ ,  $\chi = 2$  for isothermal case and  $\lambda = 3$ ,  $\chi = 2$  for constant-heat-flux case). As far as we know, only reference [9] and the present paper have tried to optimize the velocity and temperature profiles for the integral analysis of natural convection. All other references and textbooks seem to adopt, without questioning, the values  $\lambda = 3$ ,  $\chi = 2$  for all boundary conditions and all Prandtl numbers.

It is shown that for a vertical surface, the natural convective motion parallel to the surface is created due to buoyancy force, but for a horizontal surface, the natural convective motion parallel to the surface is created due to an indirect pressure difference. The governing Equation (18) or (21) derived in this paper beautifully

captures this stark difference in the mechanisms of natural convection. For a vertical surface (i.e.  $\gamma = 90^\circ$ ), the Term II in Equation (18) [or (21)], representing the indirect pressure difference, drops out and the sole cause for the generation of natural convection on a vertical surface becomes the Term III, i.e. the direct buoyancy force. For a horizontal surface (i.e.  $\gamma = 0^\circ$ ), on the other hand, the Term III in Equations (18) [or (21)], representing the buoyancy force, drops out and the sole cause for the generation of natural convection on a horizontal surface becomes the Term II, i.e. the indirect pressure difference. For surfaces at intermediate angles, both source terms (i.e. Term II and Term III) are operative, but through a comprehensive analysis we have been able to establish the generic trend in the relative magnitudes of the two source terms as a function of Grashof number, Prandtl number and inclination angle (Figs. 7–10).

In the limiting cases of vertical and horizontal surfaces, self-similar solutions exist, and Equations (14) and (15) lead to closed-form analytical relations for the Nusselt number, as given in Section 3.2. At all other intermediate values of inclination angle, the solutions are non-similar, and Equations (14) and (15) are integrated numerically.

Usually previous computational or experimental results are presented in the form of Nusselt number versus Grashof number (or Rayleigh number), with the inclination angle as a parameter. We have, however, used the inclination angle as the abscissa whenever possible. We believe this new representation of the results brings out more powerfully the role of inclination angle in determining the heat transfer rate as well as the mechanism of natural convection.

It is shown that for high Prandtl number fluids, the natural convection mechanism for vertical surface is the dominating factor for a large range of inclination angles except for near horizontal configurations. The range of inclination angles for which the vertical solution predominates decreases as the Prandtl number decreases. For very low Prandtl number fluids at low Grashof number, the vertical mechanism applies only to nearly vertical surfaces. A physical explanation for such behaviour is discovered here in terms of the relative magnitudes of the buoyancy and indirect pressure difference. Compact scaling laws for significant data reduction are proposed and explained. New algebraic correlations have been developed that give Nusselt number as explicit functions of Grashof number, Prandtl number and inclination angle, validated over the ranges  $10^3 \leq Gr \leq 10^7$ ,  $0.01 \leq Pr \leq 100$  and  $0^\circ \leq \gamma \leq 90^\circ$ .

#### Acknowledgements

The content of this paper has been enriched by the collective experience gained from various research work conducted under the guidance of Prof. A. Guha at IIT Kharagpur. The authors express their appreciation to previous students of Prof. Guha, especially D. Desamitra, P.K. Awadhiya and I. Ahamad.

#### Appendix A. Determination of the appropriate temperature and velocity profiles

##### Temperature profile

In order to solve the boundary layer equations, suppose the temperature profile is approximated by a second order polynomial of the form

$$T = C_1 + C_2y + C_3y^2. \quad (A1)$$

The boundary conditions for Equation (A1) are

$$\text{At } y = 0, \quad T = T_w(x) = T_\infty + f_1(x) \text{ or } q_w = -k \frac{\partial T}{\partial y} = f_2(x), \tag{A2a}$$

$$\text{At } y = \delta, \quad T = T_\infty, \tag{A2b}$$

$$\text{At } y = \delta, \quad \frac{\partial T}{\partial y} = 0. \tag{A2c}$$

The three conditions given by Equation (A2) are used to determine the constants  $C_1, C_2$  and  $C_3$ . The temperature distribution is obtained as,

$$\frac{\theta}{\theta_w} = \frac{T - T_\infty}{T_w - T_\infty} = \left[1 - \frac{y}{\delta}\right]^2, \tag{A3}$$

where  $\theta_w$  depends on the surface boundary condition as follows:

$$\text{For specified wall temperature, } \theta_w = f_1(x). \tag{A4a}$$

$$\text{For specified surface heat flux, } \theta_w = \frac{1}{2} f_2(x) \frac{\delta}{k}. \tag{A4b}$$

The asymptotic nature of the temperature profile at  $y = \delta$  indicates that all higher order derivatives of temperature ( $\partial^n T / \partial y^n$ ) can be set to zero at  $y = \delta$ , where  $n = 2, 3, 4, \dots$ , etc. Hence, higher order temperature profiles (e.g. cubic, quartic, etc.) can be assumed for solving the boundary layer equations, with the additional boundary conditions obtained from the above-mentioned feature (e.g.  $\partial^2 T / \partial y^2 = 0$  at  $y = \delta$  for the cubic profile). Temperature profiles obtained by assuming higher order polynomials are listed in Table A1.

**Table A1**  
Details of the temperature profiles obtained by using polynomials of different orders.

$\chi$	Temperature profile	Expression for $\theta_w$	
		Specified wall temperature	Specified surface heat flux
2	$\frac{\theta}{\theta_w} = \left[1 - \frac{y}{\delta}\right]^2$	$f_1(x)$	$\frac{1}{2} f_2(x) \frac{\delta}{k}$
3	$\frac{\theta}{\theta_w} = \left[1 - \frac{y}{\delta}\right]^3$	$f_1(x)$	$\frac{1}{2} f_2(x) \frac{\delta}{k}$
4	$\frac{\theta}{\theta_w} = \left[1 - \frac{y}{\delta}\right]^4$	$f_1(x)$	$\frac{1}{2} f_2(x) \frac{\delta}{k}$
5	$\frac{\theta}{\theta_w} = \left[1 - \frac{y}{\delta}\right]^5$	$f_1(x)$	$\frac{1}{2} f_2(x) \frac{\delta}{k}$

The method of mathematical induction is used to arrive at a generic temperature profile from the profiles listed in Table A1. The generic form of the temperature profile for a polynomial of order  $\chi$  is given by

$$\frac{\theta}{\theta_w} = \left[1 - \frac{y}{\delta}\right]^\chi, \tag{A5}$$

where  $\theta_w$  depends on the surface boundary condition as follows:

$$\text{For specified wall temperature, } \theta_w = f_1(x). \tag{A6a}$$

$$\text{For specified surface heat flux, } \theta_w = \frac{1}{\chi} f_2(x) \frac{\delta}{k}. \tag{A6b}$$

Equations (A5), (A6a) and (A6b) are the same as Equations (6),

(7a) and (7b) respectively given in the main text.

*Velocity profile*

In order to solve the boundary layer equations, suppose the velocity profile is approximated by a third order polynomial of the form

$$u = C_4 + C_5 y + C_6 y^2 + C_7 y^3. \tag{A7}$$

The boundary conditions for Equation (A7) are

$$\text{At } y = 0, \quad u = 0 \tag{A8a}$$

$$\text{At } y = \delta, \quad u = 0, \tag{A8b}$$

$$\text{At } y = \delta, \quad \frac{\partial u}{\partial y} = 0. \tag{A8c}$$

In order to determine the four constants in Equation (A7), one more boundary condition is required. This is derived by substituting Equation (9) into Equation (2), given in the main text, which gives,

$$\text{At } y = 0, \quad \frac{\partial^2 u}{\partial y^2} = -\frac{g\beta}{\nu} \left[ \frac{\cos \gamma}{(\chi + 1)} \frac{d}{dx} (\delta \theta_w) + \theta_w \sin \gamma \right] \tag{A8d}$$

Leibniz's rule has been applied in deriving Equation (A8d).

The four conditions given by Equation (A8) are used to determine the constants  $C_4, C_5, C_6$  and  $C_7$ . The velocity distribution is obtained as

$$\frac{u}{u_x} = \frac{y}{\delta} \left(1 - \frac{y}{\delta}\right)^2, \tag{A9}$$

where,

$$u_x = \frac{\delta^2}{4\nu} g\beta \left[ \frac{\cos \gamma}{(\chi + 1)} \frac{d}{dx} (\delta \theta_w) + \theta_w \sin \gamma \right]. \tag{A10}$$

The asymptotic nature of the velocity profile at  $y = \delta$  indicates that all higher order derivatives of velocity ( $\partial^n u / \partial y^n$ ) can be set to zero at  $y = \delta$ , where  $n = 2, 3, 4, \dots$ , etc. Hence, higher order velocity profiles can be assumed for solving the boundary layer equations, with the additional boundary conditions obtained from the above-mentioned feature (e.g.  $\partial^2 u / \partial y^2 = 0$  at  $y = \delta$  for the quartic profile,

$\partial^3 u / \partial y^3 = 0$  at  $y = \delta$  for a profile of order five, etc). The velocity profiles obtained by assuming different order of polynomials are listed in Table A2.

**Table A2**  
Details of the velocity profiles obtained by using polynomials of different orders.

$\lambda$	Velocity profile	Expression for $u_x$
3	$\frac{u}{u_x} = \frac{y}{\delta} \left(1 - \frac{y}{\delta}\right)^2$	$u_x = \frac{\delta^2}{24\nu} g\beta \left[ \frac{\cos \gamma}{(\chi+1)} \frac{d}{dx} (\delta\theta_w) + \theta_w \sin \gamma \right]$
4	$\frac{u}{u_x} = \frac{y}{\delta} \left(1 - \frac{y}{\delta}\right)^3$	$u_x = \frac{\delta^2}{60\nu} g\beta \left[ \frac{\cos \gamma}{(\chi+1)} \frac{d}{dx} (\delta\theta_w) + \theta_w \sin \gamma \right]$
5	$\frac{u}{u_x} = \frac{y}{\delta} \left(1 - \frac{y}{\delta}\right)^4$	$u_x = \frac{\delta^2}{80\nu} g\beta \left[ \frac{\cos \gamma}{(\chi+1)} \frac{d}{dx} (\delta\theta_w) + \theta_w \sin \gamma \right]$
6	$\frac{u}{u_x} = \frac{y}{\delta} \left(1 - \frac{y}{\delta}\right)^5$	$u_x = \frac{\delta^2}{10\nu} g\beta \left[ \frac{\cos \gamma}{(\chi+1)} \frac{d}{dx} (\delta\theta_w) + \theta_w \sin \gamma \right]$
7	$\frac{u}{u_x} = \frac{y}{\delta} \left(1 - \frac{y}{\delta}\right)^6$	$u_x = \frac{\delta^2}{12\nu} g\beta \left[ \frac{\cos \gamma}{(\chi+1)} \frac{d}{dx} (\delta\theta_w) + \theta_w \sin \gamma \right]$
8	$\frac{u}{u_x} = \frac{y}{\delta} \left(1 - \frac{y}{\delta}\right)^7$	$u_x = \frac{\delta^2}{14\nu} g\beta \left[ \frac{\cos \gamma}{(\chi+1)} \frac{d}{dx} (\delta\theta_w) + \theta_w \sin \gamma \right]$

The method of mathematical induction is used to arrive at a generic velocity profile from the profiles listed in Table A2. The generic form of the velocity profile for a polynomial of order  $\lambda$  is given by

$$\frac{u}{u_x} = \frac{y}{\delta} \left(1 - \frac{y}{\delta}\right)^{\lambda-1}, \tag{A11}$$

where,

$$u_x = \frac{\delta^2}{2(\lambda-1)\nu} g\beta \left[ \frac{\cos \gamma}{(\chi+1)} \frac{d}{dx} (\delta\theta_w) + \theta_w \sin \gamma \right]. \tag{A12}$$

Equations (A11) and (A12) are the same as Equations (10) and (11) given in the main text.

**Appendix B. Optimization of the velocity and temperature profiles for integral analysis of natural convection past a vertical surface**

As derived in Appendix A, the generalized temperature and velocity profiles for natural convection past vertical surfaces are as follows:

$$\frac{\theta}{\theta_w} = \left(1 - \frac{y}{\delta}\right)^\chi \tag{B1}$$

$$\frac{u}{u_x} = \frac{y}{\delta} \left(1 - \frac{y}{\delta}\right)^{\lambda-1} \tag{B2}$$

Textbooks on natural convection provide integral formulation only for the case  $\chi = 2, \lambda = 3$ . Reference [9] gives the mathematical details of how to formulate additional boundary conditions for higher values of  $\chi$  and  $\lambda$ , and how to solve the integral conservation equations that then arise. The procedure involves considerable algebraic manipulations; only the final results are quoted here. It is found that, like the case of horizontal surfaces described in Ref. [9], the final results for the local Nusselt number in the case of vertical surfaces can also be expressed as closed-form analytical

expressions given below as Equation (B3) for isothermal vertical surface and Equation (B4) for vertical surface with constant-heat-flux:

$$\text{Isothermal vertical surface : } Nu_{x,vt} = a_1 \left( \frac{Gr_x Pr^2}{a_2 + Pr} \right)^{1/4} \tag{B3}$$

$$\text{Constant heat flux vertical surface : } Nu_{x,vq} = a_3 \left( \frac{Gr_x^* Pr^2}{a_4 + Pr} \right)^{1/5} \tag{B4}$$

The values of the constants  $a_1$  and  $a_2$  used in Equation (B3), and  $a_3$  and  $a_4$  used in Equation (B4), depend on the choice of  $\chi$  and  $\lambda$  used, the functional dependence for a few combinations of  $\chi$  and  $\lambda$  are shown in Table B1.

**Table B1**  
The functional dependence of the constants  $a_1$  and  $a_2$  used in Equation (B3), and  $a_3$  and  $a_4$  used in Equation (B4) for a few combinations of  $\chi$  and  $\lambda$ .

$\chi$	$\lambda$	$a_1$	$a_2$	$a_3$	$a_4$
2	3	0.508	20/21	0.616	4/5
	4	0.467	5/9	0.576	7/15
	5	0.430	112/297	0.544	784/2475
	6	0.408	40/143	0.517	168/715
	7	0.386	20/91	0.494	12/65
	8	0.367	55/306	0.475	77/510
3	3	0.589	2	0.694	42/25
	4	0.548	10/9	0.655	14/15
	5	0.510	8/11	0.623	168/275
	6	0.487	75/143	0.596	63/143
	7	0.324	110/273	0.572	22/65
	8	0.440	11/34	0.552	231/850

It is found that as the order of the polynomial ( $\lambda$ ) representing the velocity profile is increased, the velocity profile becomes steeper at the surface and the velocity goes to zero more gradually at  $y = \delta$  [9,32]. A greater slope of the assumed velocity results in a lower value of the predicted Nusselt number than the actual value. Therefore, for  $Pr \ll 1$  (for which  $Nu_x$  is small), high values of  $\lambda$  improve the prediction of  $Nu_x$ . However, for  $Pr \geq 1$  (for which  $Nu_x$  is relatively greater), the Nusselt number may be under-predicted by high values of  $\lambda$ .

Different values of  $\chi$  and  $\lambda$  are used to evaluate the value of  $Nu_x / Gr_x^{1/4}$  for an isothermal surface, and some of the results obtained are tabulated alongside the results given by similarity analysis in Table B2. It is found that for  $Pr = 0.01$ , a combination of  $\chi = 3$  and  $\lambda = 6$  predicts the value of  $Nu_x / Gr_x^{1/4}$  most accurately. For  $Pr = 1$ , the prediction is most accurate when  $\chi = 2$  and  $\lambda = 4$  are used for the temperature and velocity profiles respectively. Using  $\chi = 2$  and  $\lambda = 3$  gives the best  $Nu_x / Gr_x^{1/4}$  prediction for  $Pr = 100$ . However, in order to choose the optimum velocity and temperature profiles for a range of  $Pr$ , both attaining maximum accuracy in determining  $Nu_x$  at a particular  $Pr$  and minimizing the errors incurred at all other values of  $Pr$  should be given importance. Hence, it is concluded that if a particular combination of  $\chi$  and  $\lambda$  is to be selected for the entire range of Prandtl number considered in this study ( $0.01 \leq Pr \leq 100$ ),

then the optimum choice is  $\chi = 2$  and  $\lambda = 4$ .

**Table B2**

Comparison of  $Nu_x/Gr_x^{1/4}$  obtained from the present integral analysis with those given by similarity analysis for different order polynomial approximations of the velocity and temperature for an isothermal vertical surface.

Pr	Similarity solution [1]	$\chi = 2$			$\chi = 3$		
		$\lambda = 3$	$\lambda = 4$	$\lambda = 6$	$\lambda = 3$	$\lambda = 4$	$\lambda = 6$
0.01	0.0570	0.0513	0.0539	0.0556	0.0495	0.0533	0.0569
1	0.4010	0.4298	0.4181	0.3836	0.4475	0.4546	0.4383
100	1.5470	1.6023	1.4736	1.2893	1.8534	1.7281	1.6380

A similar study is also performed for a vertical surface subjected to a constant heat flux. The values of  $Nu_x/Gr_x^{*1/5}$  obtained from the present integral analysis for a few combinations of  $\chi$  and  $\lambda$  are tabulated alongside results of similarity analysis in Table B3. It is found that for  $Pr = 0.01$ , a combination of  $\chi = 2$  and  $\lambda = 6$  predicts the value of  $Nu_x/Gr_x^{*1/5}$  most accurately. For  $Pr = 1$  and  $Pr = 100$ , the best prediction is possible by using  $\chi = 2$  and  $\lambda = 3$ . Careful observation of Table B3 shows that the improvement achieved for  $Pr = 0.01$  by using  $\lambda = 6$  is considerably smaller than the detrimental effects of such an assumption on the predictions for  $Pr = 1$  and  $Pr = 100$ . Therefore, it is concluded that for a vertical surface subjected to a constant heat flux,  $\chi = 2$  and  $\lambda = 3$  are the optimal choice for the temperature and velocity profiles respectively.

**Table B3**

Comparison of  $Nu_x/Gr_x^{*1/5}$  obtained from the present integral analysis with those given by similarity analysis for different order polynomial approximations of the velocity and temperature for a vertical surface subjected to constant heat flux.

Pr	Similarity solution [7]	$\chi = 2$			$\chi = 3$		
		$\lambda = 3$	$\lambda = 4$	$\lambda = 6$	$\lambda = 3$	$\lambda = 4$	$\lambda = 6$
0.01	0.1149	0.1018	0.1059	0.1086	0.0990	0.1050	0.1061
1	0.5479	0.5477	0.5335	0.4956	0.5698	0.5741	0.5540
100	1.5455	1.5449	1.4455	1.2980	1.7374	1.6422	1.4958

## References

- [1] Burmeister LC. Convective heat transfer. second ed. New York: John Wiley & Sons; 1993.
- [2] Kays WM, Crawford ME. Convective heat and mass transfer. third ed. New York: McGraw-Hill; 1993.
- [3] Martynenko OG, Khramtsov PP. Free convective heat transfer: with many photographs of flows and heat exchange. New York: Springer; 2005.
- [4] Sparrow EM. Laminar free convection on a vertical plate with prescribed nonuniform wall heat flux or prescribed nonuniform wall temperature. NACA TN-3508. 1955.
- [5] Pop I, Ingham DB. Convective heat transfer: mathematical and computational modelling of viscous fluids and porous media. Elsevier; 2001.
- [6] Bejan A. Convection heat transfer. fourth ed. New York: John Wiley & Sons; 2013.
- [7] Sparrow EM, Gregg JL. Similar solutions for free convection from a non-isothermal vertical plate. Trans ASME 1958;80:379–86.
- [8] Rajan VSV, Picot JJC. Experimental study of the laminar free convection from a vertical plate. Ind Eng Chem Fundam 1971;10(1):132–4.
- [9] Guha A, Samanta S. Closed-form analytical solutions for laminar natural convection on horizontal plates. ASME J Heat Transf 2013;135(10): 102501.
- [10] Amin N, Riley N. Horizontal free convection. Proceedings of the Royal Society of London A: mathematical. Phys Eng Sci 1873;1990(427):371–84.
- [11] Schlichting H, Gersten K. Boundary layer theory. eighth ed. New Delhi: Springer; 2004.
- [12] Stewartson K. On the free convection from a horizontal plate. Z Angew Math Phys 1958;9(3):276–82.
- [13] Rotem Z, Claassen L. Natural convection above unconfined horizontal surfaces. J Fluid Mech 1969;38:173–92.
- [14] Samanta S, Guha A. A similarity theory for natural convection from a horizontal plate for prescribed heat flux or wall temperature. Int J Heat Mass Transf 2012;55(13–14):3857–68.
- [15] Shapiro A, Fedorovich E. Similarity models for unsteady free convection flows along a differentially cooled horizontal surface. J Fluid Mech 2013;736: 444–63.
- [16] Goldstein RJ, Lau KS. Laminar natural convection from a horizontal plate and the influence of plate–edge extensions. J Fluid Mech 1983;129:55–75.
- [17] Clifton JV, Chapman AJ. Natural convection on a finite size horizontal plate. Int J Heat Mass Transf 1984;12(12):1573–84.
- [18] Guha A, Sengupta S. Effects of finiteness on the thermo-fluid-dynamics of natural convection above horizontal plates. Phys Fluids 2016;28(6): 063603.
- [19] Guha A, Pradhan K. Natural convection of non-Newtonian power-law fluids on a horizontal plate. Int J Heat Mass Transf 2014;70:930–8.
- [20] Rich BR, Burbank Calif. An investigation of heat transfer from an inclined flat plate in free convection. ASME J Heat Transf 1953;75:485–99.
- [21] Vliet GC. Natural convection local heat transfer on constant heat flux inclined surfaces. ASME J Heat Transf 1969;91:511–6.
- [22] Pera L, Gebhart B. Natural convection boundary layer flow over horizontal and slightly inclined surfaces. Int J Heat Mass Transf 1973;16:1131–46.
- [23] Yu WS, Lin HT. Free convection heat transfer from an isothermal plate with arbitrary inclination. Wärme-und Stoffübertragung 1988;23:203–11.
- [24] Lin HT, Yu WS, Yang SL. Free convection on an arbitrarily inclined plate with uniform surface heat flux. Wärme-und Stoffübertragung 1989;24:183–90.
- [25] Chen TS, Tien HC, Armaly BF. Natural convection on horizontal, inclined and vertical plates with variable surface temperature or heat flux. Int J Heat Mass Transf 1986;29(10):1465–78.
- [26] Saha SC, Patterson JC, Lei C. Natural convection boundary-layer adjacent to an inclined flat plate subject to sudden and ramp heating. Int J Therm Sci 2010;49(9):1600–12.
- [27] Corcione M, Habib E, Campo A. Natural convection from inclined plates to gases and liquids when both sides are uniformly heated at the same temperature. Int J Therm Sci 2011;50(8):1405–16.
- [28] Faghri A, Zhang Y, Howell J. Advanced heat and mass transfer. Columbia: Global Digital Press; 2010.
- [29] Guha A, Samanta S. Effect of thermophoresis and its mathematical models on the transport and deposition of aerosol particles in natural convective flow on vertical and horizontal plates. J Aerosol Sci 2014;77:85–101.
- [30] Ahamad I. Laminar natural convection from an inclined semi-infinite flat plate. MTech Thesis (Project Guide: A. Guha). Mechanical Engineering Department, Indian Institute of Technology Kharagpur; 2015.

- [31] Ostrach S. An analysis of laminar free convection flow and heat transfer about a flat plate parallel to the direction of the generating body force. NACA TN-2635. 1952.
- [32] Awadhiya PK. Closed-form analytical solutions for laminar natural convection from vertical flat plates. BTech Project Report (Project Guide: A. Guha). Mechanical Engineering Department, Indian Institute of Technology Kharagpur; 2014.
- [33] Churchill SW. A comprehensive correlating equation for laminar, assisting, forced and free convection. *Am Inst Chem Eng J* 1977;23(1):10–6.